

1 **Untangling irrigation effects on maize water and heat stress**
2 **alleviation using satellite data**

3

4 Peng Zhu^{1*}, Jennifer Burney¹

5 ¹School of Global Policy and Strategy, University of California, San Diego, CA USA

6 *Correspondence to:* Peng Zhu (zhuyp678@gmail.com)

7

8 **Abstract.** Irrigation has important implications for sustaining global food production,
9 enabling crop water demand to be met even under dry conditions. Added water also
10 cools crop plants through transpiration; irrigation might thus play an important role in
11 a warmer climate by simultaneously moderating water and high temperature stresses.
12 Here we used satellite-derived evapotranspiration estimates, land surface temperature
13 (LST) measurements, and crop phenological stage information from Nebraska maize
14 to quantify how irrigation relieves both water and temperature stresses. Unlike air
15 temperature metrics, satellite-derived LST revealed a significant irrigation-induced
16 cooling effect, especially during the grain filling period (GFP) of crop growth. This
17 cooling appeared to extend the maize growing season, especially for GFP, likely due
18 to the stronger temperature sensitivity of phenological development during this stage.
19 Our analysis also revealed that irrigation not only reduced water and temperature
20 stress but also weakened the response of yield to these stresses. Specifically,
21 temperature stress was significantly weakened for reproductive processes in irrigated
22 maize. Attribution analysis further suggested that water and high temperature stress
23 alleviation were responsible for $65\pm 10\%$ and $35\pm 5.3\%$ of irrigation's yield benefit,
24 respectively. Our study underlines the relative importance of high temperature stress
25 alleviation in yield improvement and the necessity of simulating crop surface
26 temperature to better quantify heat stress effects in crop yield models. Finally,
27 untangling irrigation's effects on both heat and water stress mitigation has important
28 implications for designing agricultural adaptation strategies under climate change.

29

30 **Keywords:** Irrigation, Evaporative cooling, MODIS LST, High temperature
31 stress, Water stress, Maize

32

33 **1. Introduction**

34 Irrigation -- a large component of freshwater consumption sourced from water
35 diversion from streams and groundwater (Wallace, 2000, Howell, 2001) -- allows
36 crops to grow in environments that do not receive sufficient rainfall, and buffers
37 agricultural production from climate variability and extremes. Irrigated agriculture
38 plays an outsized role in global crop production and food security: irrigated lands
39 account for 17% of total cropped area, yet they provide 40% of global cereals
40 (Rosegrant et al 2002, Siebert and Döll 2010). Meeting the rising food demands of a
41 growing global population will require either increasing crop productivity and/or
42 expansion of cropped areas; both strategies are daunting under projected climate
43 change. Cropland expansion may be in marginal areas that require irrigation even in
44 the present climate (Bruinsma 2009); increasing temperatures will drive higher
45 atmospheric vapor pressure deficits (VPD) and raise crop water demand and crop
46 water losses. This increasing water demand poses a water ceiling for crop growth and
47 might necessitate irrigation application over present rainfed areas to increase or even
48 maintain yields (DeLucia et al., 2019).

49

50 However, the provision of additional irrigation water modifies both the land surface
51 water and energy budgets. Additional water can result in an evaporative cooling
52 effect, which may be beneficial for crop growth indirectly through lowering the
53 frequency of extreme heat stress (Butler et al., 2018). High temperature stress will be
54 more prevalent (Russo et al., 2014) under future warming, and might result in more
55 severe yield losses than water stress (Zhu et al., 2019) due to reduced photosynthesis,
56 pollen sterility, and accelerated crop senescence in major cereals (Rezaei et al.,
57 2015b; Rattalino Edreira et al., 2011; Ruiz-Vera et al., 2018). A better understanding
58 of irrigation's potential to alleviate high temperature stress will therefore be important
59 for agricultural management. More broadly, understanding how irrigation can or
60 should contribute to a portfolio of agricultural adaptation strategies thus requires
61 improved understanding of its relative roles in mitigating both water and heat stresses.

62

63 Climate models and meteorological data have been used to investigate how historical
64 expansion of irrigation at global and regional scales has influenced the climate
65 system, including surface cooling and precipitation variation (Kang and Eltahir, 2019;

66 Thiery et al., 2017; Bonfils and Lobell, 2007; Sacks et al., 2009). However, many
67 crop models still use air temperature rather than canopy temperature to estimate heat
68 stress; this may overestimate heat stress effects in irrigated cropland (Siebert et al.,
69 2017), since canopy temperature can deviate significantly from air temperature
70 depending on the crop moisture conditions (Siebert et al., 2014). Recently, a
71 comparison of crop model simulated canopy temperatures suggests that most crop
72 models lack a sufficient ability to reproduce the field-measured canopy temperature,
73 even for models with a good performance in grain yield simulation (Webber et al.,
74 2017).

75

76 Satellite-derived land surface temperature (LST) measurements have been used to
77 directly quantify regional scale surface warming or cooling effects resulting from
78 surface energy budget changes due to changes in land cover and land management
79 (Loarie et al., 2011; Tomlinson et al., 2012; Peng et al., 2014). Importantly, yield
80 prediction model comparisons suggest that replacing air temperature with MODIS
81 LST can improve yield predictions because LST accounts for both evaporative
82 cooling and water stress (Li et al., 2019). Satellite data also provide the observational
83 evidence to constrain model performance or directly retrieve crop growth status
84 information. For example, satellite derived soil moisture had been used to characterize
85 irrigation patterns and improve irrigation quantity estimations (Felfelani et al., 2018;
86 Lawston et al., 2017; Jalilvand et al., 2019; Zaussinger et al., 2019). Integration of
87 satellite products like LST therefore have the potential to improve our understanding
88 of how irrigation and climate change impact crop yields, and thus provide guidance
89 for farmers to optimize management decisions.

90

91 In this study, we focused on Nebraska, the third largest maize producer in the United
92 States. Multi-year mean climate data showed that conditions have been drier in
93 western areas and warmer in southern areas of the state (Figure 1a and b).
94 Importantly, Nebraska has historically produced a mixture of irrigated and rainfed
95 maize that facilitated comparison (more than half (56%) of the Nebraska maize
96 cropland was irrigated, with more irrigated maize in the western area (Figure 1c),
97 according to the United States Department of Agriculture (USDA, 2018a)). County
98 yield data from the USDA showed that interannual fluctuations in rainfed maize yield
99 have in general been much larger than for irrigated maize (Figure 1b). Although

100 irrigated yields were higher, rainfed maize yields have grown faster than irrigated (an
101 average of 3.9% per year versus 1.0% per year) over the study period (2003-2016)
102 (Figure 1b), in part because breeding technology progress has improved the drought
103 tolerance of maize hybrids (Messina et al., 2010).

104

105 As noted above, irrigation potentially benefits crop yields by moderating both water
106 and high temperature stress. Here we used satellite-derived LST and satellite-derived
107 water stress metrics to statistically tease apart the contributions of irrigation to water
108 and heat stress alleviation, separately. We: (1) evaluated the difference in temperature
109 and moisture conditions over irrigated and rainfed maize croplands; (2) explored how
110 irrigation mitigated water and high temperature stresses using panel statistical models;
111 (3) quantified the relative contributions of irrigation-induced water and high
112 temperature stress alleviation to yield improvements; and (4) explored whether
113 current crop models reproduced the observed irrigation benefits on maize growth
114 status.

115 **2. Materials and Methods**

116 We first describe the data used, followed by a brief description of statistical
117 methodology.

118 **2.1 Satellite products to identify irrigated and non-irrigated maize areas**

119 We used the United States Department of Agriculture's Cropland Data Layer (CDL)
120 to identify maize croplands for each year in the study period 2003-2016 (USDA,
121 2018b). The irrigation distribution map across Nebraska was obtained from a previous
122 study that used Landsat-derived plant greenness and moisture information to create a
123 continuous annual irrigation map across U.S. Northern High Plains (Deines et al.,
124 2017). The irrigation map showed a very high accuracy (92 to 100%) when validated
125 with randomly generated test points and also highly correlated with county statistics
126 ($R^2 = 0.88-0.96$) (Deines et al., 2017). Both the CDL and irrigation map are at 30m
127 resolution. We first projected them to MODIS sinusoidal projection and then
128 aggregated them to 1km resolution to align with MODIS ET and LST products. Then,
129 pixels containing more than 60% maize and an irrigation fraction >60% were labeled
130 as irrigated maize while pixels with >60% maize and <10% irrigation fraction were
131 labeled as rainfed maize croplands. As always, threshold selection involves a tradeoff

132 between mixing samples and retaining as many samples as possible. Our choices of
133 <10% as the threshold for rainfed maize and 60% to define irrigated maize
134 represented the best optimization in our sample, as we found that more stringent
135 threshold had a very small effect on LST differences between irrigated and rainfed
136 maize at county level but resulted in significant data omission (more details in
137 supplementary Figure 1-2).

138 **2.2 Maize phenology information**

139 Maize growth stage information derived in a previous study was used to assess the
140 influence of irrigation on maize growth during different growth stages (Zhu et al.,
141 2018). Stage information including emergence date, silking date, and maturity date,
142 was derived with MODIS WDRVI (Wide Dynamic Range Vegetation Index, 8-day
143 and 250m resolution) based on a hybrid method combining shape model fitting (SMF)
144 and threshold-based analysis. Then we defined vegetative period (VP) as period from
145 emergence date to silking date, grain filling period (GFP) as period from silking date
146 to maturity date and growing season (GS) as period from emergence date to maturity
147 date. Details can be found in our previous studies (Zhu et al., 2018). WDRVI was
148 used due to its higher sensitivity to changes at high biomass than other vegetation
149 indices (Gitelson et al., 2004) and was estimated with the following equation:

$$150 \quad NDVI = (\rho_{NIR} - \rho_{red}) / (\rho_{NIR} + \rho_{red}) \quad (1)$$

$$151 \quad WDRVI = 100 * \frac{[(\alpha - 1) + (\alpha + 1) \times NDVI]}{[(\alpha + 1) + (\alpha - 1) \times NDVI]} \quad (2)$$

152 where ρ_{red} and ρ_{NIR} were the MODIS surface reflectance in the red and NIR bands,
153 respectively. To minimize the effects of aerosols, we used the 8-day composite
154 products in MOD09Q1 and MYD09Q1 and quality-filtered the reflectance data using
155 the band quality control flags. Only data passing the highest quality control were
156 retained (Zhu et al., 2018). The scaling factor, $\alpha=0.1$, was adopted based on a
157 previous study to degrade the fraction of the NIR reflectance at moderate-to-high
158 green vegetation and best linearly capture the maize green leaf area index (LAI)
159 (Guindin-Garcia et al., 2012).

160 **2.3 Temperature exposure during maize growth**

161 We used daily 1-km spatial resolution MODIS Aqua LST (MYD11A1) data to
162 characterize the crop surface temperature; since its overpassing times are at 1:30 and
163 13:30, it is closer to the times of daily minimum and maximum temperature than the

164 MODIS Terra LST (Wan et al., 2008) and is therefore better for characterizing crop
 165 surface temperature stress (Johnson 2016; Li et al., 2019). For quality control, pixels
 166 with an LST error >3 degree were filtered out based on the corresponding MODIS
 167 LST quality assurance layers. Missing values (less than 3% of total observations)
 168 were interpolated with robust spline function (Teuling et al., 2010). Aqua LST data
 169 are available after July 2002; we thus restricted our study to the period 2003-2016.
 170 For comparison, we also obtained daily minimum and maximum surface air
 171 temperature (Tmin and Tmax) at 1-km resolution from Daymet version 3 (Thornton et
 172 al., 2018). For both MODIS LST and air temperature, we calculated integrated crop
 173 heat exposure -- the growing degree days (GDD) and extreme degree days (EDD) --
 174 according to the following definitions:

175

$$176 \quad GDD_8^{30} = \sum_{t=1}^N DD_t, \quad DD_t = \begin{cases} 0, & \text{when } T < 8^{\circ}\text{C} \\ T - 8, & \text{when } 8^{\circ}\text{C} \leq T < 30^{\circ}\text{C} \\ 22, & \text{when } T \geq 30^{\circ}\text{C} \end{cases} \quad (3)$$

$$177 \quad EDD_{30}^{\infty} = \sum_{t=1}^N DD_t, \quad DD_t = \begin{cases} 0, & \text{when } T < 30^{\circ}\text{C} \\ T - 30, & \text{when } T \geq 30^{\circ}\text{C} \end{cases} \quad (4)$$

178 Here temperature (T) could be either air temperature or LST, interpolated from daily
 179 to hourly values with sine function (Tack et al., 2017). t represents the hourly time
 180 step, N is the total number of hours in a specified growing period (either the entire
 181 growing season, or a specific phenological growth phase, as defined below).
 182 Following previous studies (Lobell et al., 2011; Zhu et al., 2019), we used 30 °C as the
 183 high temperature threshold, although higher values might be applicable in some
 184 settings (Sanchez et al., 2014).

185

186 **2.4 Maize Water Stress**

187 Water stress during maize growth was characterized by the ratio of evapotranspiration
 188 (ET) to potential evapotranspiration (PET), as in a previous study (Mu et al., 2013).
 189 We used MODIS products (MYD16A2) for both ET and PET, based on its good
 190 performance for natural vegetation (Mu et al., 2011); however, our comparison using
 191 flux tower observed ET at an irrigated maize site at Nebraska suggested that ET at the
 192 irrigated maize was significantly underestimated by MODIS ET (Supplementary
 193 Figure 3). We therefore also used another ET product (SSEBop ET) to replace

194 MODIS ET. SSEBop ET was also estimated with MODIS products (Senay et al.,
195 2013), like LST, vegetation index, and albedo as input variables, but used a revised
196 algorithm including predefined boundary conditions for hot and cold reference pixels
197 (Senay et al., 2013) and showed better performance than MODIS ET (Velpuri et al.,
198 2013). We also saw improved performance when we compared it with flux tower
199 observed ET at an irrigated maize site (Supplementary Figure 4). The comparison of
200 MODIS PET and flux tower estimated PET showed satisfactory performance for
201 MODIS PET (Supplementary Figure 5). Since MODIS PET from MYD16A2 has a
202 spatial resolution of 500 m with 8-day temporal resolution, while SSEBop ET has
203 1km spatial resolution with daily time step, we reconciled the two datasets to 1km
204 spatial resolution and 8-day temporal resolution.

205 **2.5 Crop model simulation results**

206 We compared the results of our statistical analysis with four gridded crop models.
207 Simulation results from pAPSIM, pDSSAT, LPJ-GUESS, CLM-crop for both rainfed
208 and irrigated maize across Nebraska were obtained from Agricultural Model
209 Intercomparison and Improvement Project (AgMIP) (Rosenzweig et al., 2013) and
210 Inter-Sectoral Impact Model Intercomparison Project 1 (ISIMIP1) (Warszawski et al.,
211 2014). The four models were driven by the same climate forcing dataset (AgMERRA)
212 and run at a spatial resolution of 0.5 arc-degree longitude and latitude. All simulations
213 were conducted for purely rainfed and near-perfectly irrigated conditions. These
214 models simulated maize yield, total biomass, ET and growing stage information
215 (planting date, flowering date and maturity date). Planting date occurs on the first day
216 following the prescribed sowing date in which soil temperature is at least 2 degrees
217 above the 8 °C base temperature. Harvest occurs once the specified heat units are
218 reached. Heat units to maturity were calibrated from the prescribed crop calendar data
219 (Elliott et al., 2015). Crop model simulation was evaluated by calculating the Pearson
220 correlation between simulated yields in the baseline simulations and detrended
221 historical yields for each country from the Food and Agriculture Organization.
222 Management scenario ‘harmon’ was selected, meaning the simulation using
223 harmonized fertilizer inputs and assumptions on growing seasons. More details on the
224 simulation protocol can be found in Elliott et al. (2015) and Müller et al. (2019). We
225 used this model comparison project outputs to shed light on how well crop models
226 had simulated the irrigation benefits we identified in different phases of crop growth.

227 **2.6 Method**

228 We used standard panel statistical analysis techniques to identify the impacts of
229 irrigation on maize productivity via heat stress reduction and water stress reduction
230 pathways.

231

232 Comparison of LST, ET, PET, ET/PET, GDD and EDD between irrigated and rainfed
233 maize areas was performed within each county to minimize the effects of other
234 spatially-varying factors, like background temperature and management practices, on
235 surface temperature and evapotranspiration. These biophysical variables (LST, ET,
236 PET, ET/PET, GDD and EDD) averaged over each county were then integrated over
237 vegetative period (VP, from emergence date to silking date), grain filling period (GFP,
238 from silking date to maturity date) and whole growing season (GS, from emergence
239 date to maturity date) so we could evaluate whether and how irrigation had
240 differentially influenced maize growth during early VP and late GFP.

241

242 We further examined how irrigation had changed the sensitivity of maize yield and its
243 components to temperature variation. As done in our previous study (Zhu et al., 2019),
244 we decomposed the total yield variation into three components: biomass growth rate
245 (BGR), growing season length (GSL) and harvest index (HI) based on the following
246 equation:

$$247 \text{Yield} = HI \cdot AGB = HI \cdot BGR \cdot GSL \quad (5)$$

248 Aboveground biomass (AGB) was retrieved through a regression model:

$$249 \text{AGB} = 16.4 \cdot \text{IWDRVI}^{0.8} \quad (6)$$

250 which was built in the previous study through regressing field measured maize AGB
251 against MODIS derived integrated WDRVI (IWDRVI) (Zhu et al., 2019). Then HI
252 could be estimated as Yield/AGB and BGR could be estimated as AGB/GSL. This
253 decomposition allowed us to examine how different crop growth physiological
254 processes responded to external forcing: HI characterizes dry matter partitioning
255 between source organ and sink organ and is mainly related with processes
256 determining grain size and grain weight; BGR is related with physiological processes
257 of daily carbon assimilation rate through photosynthesis and GSL is related with crop
258 phenological development. The uncertainties in AGB estimation results from the
259 parameters in the regression model (Eq. (6)) converting IWDRVI to AGB. Here we
260 quantified the uncertainties rooted in the estimated parameters through running the

261 panel model 1000 times with the samples generated from each parameter's 95%
 262 confidence interval (Zhu et al., 2019).

263

264 Temperature sensitivity of irrigated or rainfed yield (S_T^{Yield}) was estimated using a
 265 panel data model (Eq. (7)) with growing season mean LST and ET/PET as the
 266 explanatory variables:

$$267 \log(Yield_{i,t}) = \gamma_1 t + \gamma_2 LST_{i,t} + \gamma_3 \frac{ET}{PET_{i,t}} + County_i + \varepsilon_{i,t} \quad (7)$$

268 $Yield_{i,t}$ is maize yield (t/ha) in county i and year t . It is a function of overall yield
 269 trends ($\gamma_1 t$) that have fairly steadily increased over the study period (Figure 1b), local
 270 crop temperature stress ($LST_{i,t}$), and local crop water stress ($\frac{ET}{PET_{i,t}}$). The $County_i$
 271 terms provide an independent intercept for each county (fixed effect), and thus
 272 account for time-invariant county-level differences that contributed to variations in

$\frac{\partial \ln(Yield)}{\partial LST}$

273 yield, like the soil quality. $\varepsilon_{i,t}$ is an idiosyncratic error term. γ_2 or $\frac{\partial \ln(Yield)}{\partial LST}$ defines
 274 the temperature sensitivity of yield. The temperature sensitivity of BGR (S_T^{BGR}), HI
 275 (S_T^{HI}) and GSL (S_T^{GSL}) could be estimated with Eq (7) in a similar way through using
 276 BGR, HI and GSL as the dependent variable. Here the dependent variable Yield
 277 (BGR, GSL and HI) was logged, so the estimated temperature sensitivity represented
 278 the percentage change of Yield (BGR, GSL and HI) with 1 °C temperature increase.

279

280 To quantify the relative contribution of water and high temperature stress alleviation
 281 to yield benefit, we related the yield difference between irrigated and non-irrigated
 282 maize (irrigation yield-rainfed yield, $\Delta Yield$) to a quadratic function of growing
 283 season EDD and ET/PET differences between irrigated and rainfed maize:

$$284 \Delta Yield_{i,t} = \gamma_1 \Delta \frac{ET}{PET_{i,t}} + \gamma_2 \Delta \frac{ET}{PET_{i,t}}^2 + \gamma_3 \Delta EDD_{i,t} + \gamma_4 \Delta EDD_{i,t}^2 + County_i + \varepsilon_{i,t} \quad (8)$$

285 The yield improvement explained by heat and water stress alleviation was estimated

$$286 \text{ as } \frac{\gamma_1 \sum \Delta \frac{ET}{PET_{i,t}} + \gamma_2 \sum \Delta \frac{ET}{PET_{i,t}}^2 + \gamma_3 \sum \Delta EDD_{i,t} + \gamma_4 \sum \Delta EDD_{i,t}^2}{\sum \Delta Yield_{i,t}} \quad . \quad \text{The relative}$$

287 contribution of water and high temperature stress alleviation was estimated as

$$\frac{\gamma_1 \sum \Delta \frac{ET}{PET_{i,t}} + \gamma_2 \sum \Delta \frac{ET^2}{PET_{i,t}}}{\gamma_1 \sum \Delta \frac{ET}{PET_{i,t}} + \gamma_2 \sum \Delta \frac{ET^2}{PET_{i,t}} + \gamma_3 \sum \Delta EDD_{i,t} + \gamma_4 \sum \Delta EDD_{i,t}^2}$$

288 and

$$\frac{\gamma_3 \sum \Delta EDD_{i,t} + \gamma_4 \sum \Delta EDD_{i,t}^2}{\gamma_1 \sum \Delta \frac{ET}{PET_{i,t}} + \gamma_2 \sum \Delta \frac{ET^2}{PET_{i,t}} + \gamma_3 \sum \Delta EDD_{i,t} + \gamma_4 \sum \Delta EDD_{i,t}^2},$$

289 respectively. We also

290 ran the model above using daytime LST difference (ΔLST) in lieu of ΔEDD as a
291 robustness check:

$$\Delta Yield_{i,t} = \gamma_1 \Delta \frac{ET}{PET_{i,t}} + \gamma_2 \Delta \frac{ET^2}{PET_{i,t}} + \gamma_3 \Delta LST_{i,t} + \gamma_4 \Delta LST_{i,t}^2 + County_i + \varepsilon_{i,t} \quad (9)$$

292

293 To diagnose any potential collinearity between $\Delta \frac{ET}{PET}$ and ΔLST , we calculated the
294 Variance Inflation Factor (VIF) for the model above. In this formulation the relative
295 contributions of water and high temperature stress alleviation were estimated as

$$\frac{\gamma_1 \sum \Delta \frac{ET}{PET_{i,t}} + \gamma_2 \sum \Delta \frac{ET^2}{PET_{i,t}}}{\gamma_1 \sum \Delta \frac{ET}{PET_{i,t}} + \gamma_2 \sum \Delta \frac{ET^2}{PET_{i,t}} + \gamma_3 \sum \Delta LST_{i,t} + \gamma_4 \sum \Delta LST_{i,t}^2}$$

296 and

$$\frac{\gamma_3 \sum \Delta LST_{i,t} + \gamma_4 \sum \Delta LST_{i,t}^2}{\gamma_1 \sum \Delta \frac{ET}{PET_{i,t}} + \gamma_2 \sum \Delta \frac{ET^2}{PET_{i,t}} + \gamma_3 \sum \Delta LST_{i,t} + \gamma_4 \sum \Delta LST_{i,t}^2},$$

297 respectively.

298 3. Results

299 As expected, irrigation improved maize yield and the yield benefit showed a distinct
300 spatial variation when we compared areas we identified as irrigated versus rainfed
301 maize. The yield benefit of irrigation was much higher in the western area of the state
302 (Figure 2a), because the drier environment in western area featured a wider yield gap
303 between irrigated and rainfed cropland in an average year. The satellite derived
304 vegetation index WDRVI reflected these differences, with higher values in areas we
305 identified as irrigated maize, especially around maize silking (Figure 2b). Importantly,
306 this suggested that irrigated and rainfed cropland were distinguishable based on
307 satellite derived crop seasonality information.

308

309 When county-level LST data were averaged over 2003-2016, the daytime LST in
310 irrigated maize was 1.5°C cooler than rainfed maize, while nighttime LST showed a
311 very slight difference (0.2°C) (Figure 3a,b). When the LST differences were
312 integrated over different growing periods (Figure 3e-h), we found that the daytime
313 cooling effect was greatest in the GFP (Figure 3g), probably due to the higher LAI (or
314 ground cover) and transpiration during that stage of growth. This was also consistent
315 with previous field studies showing that irrigation was mainly applied during the
316 middle to late reproductive period, which corresponded to the greatest water demand
317 period (Chen et al., 2018). The spatial pattern of the LST difference showed stronger
318 cooling effect in the western area (Figure 3c-h), which was similar to the spatial
319 pattern of yield benefit identified in Figure 2a. In contrast, surface air temperature
320 showed much smaller daytime cooling effect (Figure 3i,j). The mean daytime and
321 nighttime air temperature differences between irrigated and rainfed maize were -0.2°C
322 and -0.3°C, respectively, and the spatial pattern of air temperature difference over VP
323 and GFP was also relatively small between counties and crop growth periods (Figure
324 3k-p). The difference between spatial-temporal patterns identified using LST and air
325 temperature likely arises because LST reflects canopy energy partition between latent
326 heat flux and sensible heat flux. Additional moisture provided by irrigation results in
327 more heat transferred as latent heat flux, creating a cooling effect.

328

329 Temperature is an important driver of crop phenology and has been used as the
330 primary environmental variable in crop phenology models (Wang et al., 1998). Given
331 the identified irrigation cooling, we further examined how irrigation altered maize
332 phenological stages. We found irrigated maize showed an earlier emergence and
333 silking but delayed maturity (Figure 4a). Consequently, GFP was extended by 7.5
334 days on average, which contributed to most of the total GS extension (8.1 days)
335 (Figure 4b). Site measurements of phenological stage information confirmed that
336 irrigated maize had a longer GS, especially during GFP (Figure 4c). That this
337 extension mainly occurred during GFP could be due to: (1) LST cooling was more
338 prominent during GFP and (2) phenological development during GFP was more
339 sensitive to temperature variation than development during VP (Egli et al., 2004). The
340 higher temperature sensitivity of phenological development during GFP (4.9 day/°C)
341 was supported by a regression model relating the GFP difference between irrigated
342 and rainfed maize to the LST difference between irrigated and rainfed maize (Figure

343 4d-f). The spatial pattern suggested GS and GFP extension were more significant in
344 the western area of the state (Figure 4g-h), likely due to the corresponding stronger
345 cooling effect.

346

347 We integrated LST or air temperature as described above (Materials and Methods) to
348 estimate total heat exposure (GDD and EDD) over the maize growing season. We
349 found both LST and air temperature estimated GDD were greater in irrigated maize
350 than GDD in rainfed maize across most counties, especially during GFP (Figure 5a,c),
351 which was very likely due to the GFP extension. As GDD characterizes the beneficial
352 thermal time accumulation, the greater GDD in irrigated maize might contribute to the
353 higher yield. In terms of EDD, LST estimated EDD suggested that irrigation
354 suppressed high temperature stress especially for GFP (Figure 5b), while air
355 temperature estimated EDD failed to characterize the irrigation induced lower high
356 temperature stress (Figure 5d).

357

358 SSEBop ET and MODIS PET were used to explore how irrigation influenced water
359 demand and water supply across maize. We found irrigation led to 27% higher ET
360 and 2% lower PET (Figure 6a-b). Higher ET was anticipated in irrigated maize, and
361 lower PET might be due to irrigation cooling effect, which resulted in lower VPD and
362 thus lower evaporative demand. We used the ratio of ET to PET as a proxy for water
363 stress in this study, where low values indicated that plants were not transpiring at their
364 full potential in the ambient conditions. This ratio was higher for irrigated maize,
365 especially during the GFP (Figure 6c), and the spatial distribution suggested that the
366 difference was greater in western counties than eastern counties (Figure 6d-e), similar
367 to the distribution of the local cooling effect identified in Figure 3c.

368

369 We divided the temperature sensitivity of yield into three components (sensitivity of
370 BGR, GSL and HI) to investigate how irrigation changed the response of maize
371 physiological processes to temperature. As shown in Figure 7, we found that
372 temperature sensitivity of yield was significantly weakened from $-6.9\%/^{\circ}\text{C}$ to $-1\%/^{\circ}\text{C}$
373 in rainfed vs. irrigated areas, and this yield sensitivity change was mainly driven by a
374 change in the sensitivity of the HI, which was weakened from $-4.2\%/^{\circ}\text{C}$ to $1\%/^{\circ}\text{C}$. In
375 both rainfed and irrigated maize, temperature sensitivity of GSL was quite close

376 (approximately $-2\%/^{\circ}\text{C}$), while BGR was only slightly influenced by temperature
377 (Figure 7).

378

379 We found that irrigation not only lowered water and high temperature stress, but also
380 made yield less sensitive to water and high temperature stress (Figure 8a-c),
381 consistent with previous studies (Troy et al., 2015; Tack et al., 2017). We statistically
382 related yield differences to climatic variables differences using the linear model (Eq.
383 (8)), and estimated that $61 \pm 9.4\%$ of yield improvement between irrigated and rainfed
384 maize could be explained by the irrigation induced heat and water stress alleviation.
385 We further calculated that $79 \pm 13\%$ of that yield improvement was due to water stress
386 alleviation and $21 \pm 3.2\%$ was due to heat stress alleviation. Because the distribution of
387 ΔEDD was truncated for points with $\Delta\text{EDD} > 0$ (Figure 8e), we explored an alternative
388 model with quadratic functions of ΔLST and $\Delta\text{ET}/\text{PET}$ (Eq. (9)). In this specification,
389 $72 \pm 12\%$ of yield improvement was explained by water and high temperature stress
390 alleviation, with $65 \pm 10\%$ and $35 \pm 5.3\%$ of yield improvement due to water and high
391 temperature stress alleviation, respectively. Because collinearity between ΔLST and
392 $\Delta\text{ET}/\text{PET}$ was potentially worrisome, we quantified the variance inflation factor (VIF)
393 in the model; this was found to be well below standard thresholds, with a value of 2.2
394 (VIFs over 10 indicate strongly collinear variables, with 5 being a more strict
395 standard). Intuitively, our low VIF value was likely due to the use of differences in
396 LST and ET/PET between irrigated and rainfed maize, rather than directly using LST
397 and ET/PET as the explanatory variables. We also note that the high temperature
398 stress alleviation estimated here appears larger than the estimation in a recent study
399 (Li et al., 2020) where LST was also employed to detect the yield benefit of irrigation
400 cooling effect. But this is due to the fact that we estimated cooling effect benefits
401 relative to total sum of cooling and water stress effects, whereas Li et al. calculated
402 cooling effect relative to net yield differences between irrigated and rainfed maize.
403 Since other effects (like cultivar difference and fertilizer application) might also
404 contribute to the yield difference between irrigated and rainfed maize, the
405 denominator used in Li et al., (2020) was larger.

406

407 Because we found a strong effect on yields via alleviation of heat stress (and not
408 simply water stress), we compared our results with four process-based crop models
409 that simulated crop growth under both rainfed and irrigated conditions. These

410 simulations qualitatively reproduced the irrigation-induced higher maize yield,
411 biomass, and ET (Figure 9), but to different degrees. The highest modeled
412 improvement was identified in CLM-crop, with increases of 57%, 43% and 32% in
413 yield, biomass and ET, respectively. However, all models except CLM-crop failed to
414 reproduce the growing stage extension under irrigation (Figure 9), likely because
415 CLM-crop was the only one of the tested models to have implemented a canopy
416 energy balance module to simulate canopy temperature. CLM-crop was thus the only
417 model able to capture the irrigation-induced evaporative cooling effect (heat-stress
418 reduction). That the best agreement between observed and modeled results occurred
419 with the only model that plausibly accounted for heat-stress alleviation due to
420 irrigation was further evidence that this was the phenomenon we captured in our
421 satellite observational study.

422 **4. Discussion and conclusion**

423 By integrating satellite products and ground-based information on cropping and
424 irrigation, we showed that irrigated maize yields were higher than rainfed maize
425 yields because added irrigation water reduced heat stress in addition to water stress.
426 Our study underlines the relative importance of heat stress alleviation in yield
427 improvement and the necessity of incorporating crop canopy temperature models to
428 better characterize heat stress impacts on crop yields (Teixeira et al., 2013; Kar and
429 Kumar, 2007). Our analysis disentangling the relative importance of heat and water
430 stress alleviation in yield benefit can help farmers plan future investments, especially
431 in terms of selecting cultivars with heat or drought stress tolerance. In addition,
432 disentangling the two effects allows crop models to better predict crop phenology,
433 considering irrigation induced cooling effect alters maize growing phases.

434

435 Although ours is not the first study to suggest replacing air temperature with MODIS
436 LST for maize yield prediction, especially under extreme warm and dry conditions,
437 our results underscore important implications of doing so. Given the important role of
438 heat stress in determining crop yield, thermal band derived LST information at finer
439 spatial and temporal resolution should be a critical input for satellite data driven yield
440 prediction models (Wang et al., 2015; Huryňa et al., 2019; Li et al., 2019; Meerdink et
441 al., 2019). In addition, given the differential responses of crop growth to heat and

442 water stresses in different stages, fusing satellite derived crop stage information with
443 the heat and water stressors might improve crop yield prediction.

444

445 This study also has useful implications for process-based crop model development. In
446 our model evaluation, only the model that had implemented a canopy energy balance
447 scheme captured the observed maize growth stage extension. Our results suggest that
448 the heat stress alleviation due to irrigation identified here is largely overlooked in
449 current crop models. As such, when those crop models are calibrated to match
450 observed yields, processes associated with water stress alleviation are probably
451 overestimated, resulting in uncertainties for predicting future irrigation water demand
452 and crop yield. These uncertainties might mislead future adaptation decisions due to
453 incomplete or biased estimates of the relative contributions of heat and water stress.
454 Relatedly, recent studies identified a wide range for the simulated canopy temperature
455 in current crop models (Webber et al., 2017). Therefore, assimilating satellite derived
456 LST might be a potential solution to improving crop models heat stress representation
457 so that they can better reproduce the observed heat stress effects (Meng et al., 2009;
458 Xu et al., 2011). These remotely sensed LST can also be used to validate model
459 simulated LST, especially given that the recent ECOSystem Spaceborne Thermal
460 Radiometer Experiment on Space Station (ECOSTRESS) mission makes hourly plant
461 temperature measurement available (Meerdink et al., 2019). However, it is worth
462 noting that the availability of satellite LST presents a constraint when thinking about
463 future climate change impact studies. In addition, some caution is required for
464 validating model-simulated LST, since LST is sensor- and satellite- specific.

465

466 Several limitations and caveats apply to our study. First, the daily MODIS daytime
467 LST we used to explain crop maximum daily temperature had missing values due to
468 quality control checks, and was derived from a mix of crop covers and other land
469 surface temperature information, which might bias the identified irrigation cooling
470 effect. Specifically, using MODIS daytime LST as a proxy for true (measured)
471 maximum crop surface temperature in an empirical statistical model might
472 underestimate the benefit of cooling effect (measurement error in a predictor variable
473 producing attenuation bias). These uncertainties in LST dataset might be resolved
474 with the recently launched ECOSTRESS mission, as its hourly revisiting frequency
475 enables better estimation of maximum daily temperature. The second issue is that

476 water stress and heat stress are not perfectly separable. As what we have shown, the
477 cooling effect of irrigation lowers evaporative demand (PET) and thus indirectly
478 contributes to lower water stress (higher ET/PET). In addition, water stress reduced
479 photosynthesis and ET, resulting in higher plant temperature. Our disentangling
480 methods do not account for the water stress and heat stress interaction effects, so these
481 “heat” and “water stress” channels should be interpreted carefully. We note that our
482 statistical model estimated temperature coefficient should be interpreted as the net of
483 all effects raising surface temperature. The third issue is that our study only examined
484 maize in one state, Nebraska. Although Nebraska is the largest irrigated maize
485 producer in the US, results might differ for other crop types and other landscapes, due
486 to different crop canopy structures and management practices (Chen et al., 2018), and
487 spatial variations in water and heat stresses mitigation effects (Figure 3 and Figure 7).

488

489 Overall, our study suggests that heat stress alleviation, in addition to water stress
490 alleviation, plays an important role in improving irrigated maize yield. Since current
491 models generally cannot accurately simulate the canopy temperature, the irrigation
492 induced yield benefit might have been overly attributed to water stress alleviation.
493 This might bias the future yield prediction under irrigation, since high temperature
494 stress might be more dominant than drought for crop yield formation under future
495 warmer climate (Zhu et al, 2019; Jin et al., 2017). Better constrained crop models --
496 perhaps through integration of satellite observed land surface temperature and crop
497 stage information -- will be necessary to improve yield prediction and help
498 policymakers and farmers make better decisions about where and when to implement
499 irrigation.

500

501 **References**

- 502 Autovino, D., Minacapilli, M. and Provenzano, G.: Modelling bulk surface resistance
503 by MODIS data and assessment of MOD16A2 evapotranspiration product in an
504 irrigation district of Southern Italy, *Agric. Water Manag.*, 167, 86–94,
505 doi:10.1016/j.agwat.2016.01.006, 2016.
- 506 Bonfils, C. and Lobell, D.: Empirical evidence for a recent slowdown in irrigation-
507 induced cooling, *Proc. Natl. Acad. Sci. U. S. A.*, 104(34), 13582–13587,
508 doi:10.1073/pnas.0700144104, 2007.
- 509 Bruinsma, J.: The resource outlook to 2050: by how much do land, water and crop
510 yields need to increase by 2050?
511 <ftp://ftp.fao.org/docrep/fao/012/ak971e/ak971e00.pdf>, 2009.
- 512 Chen, F., Xu, X., Barlage, M., Rasmussen, R., Shen, S., Miao, S. and Zhou, G.:
513 Memory of irrigation effects on hydroclimate and its modeling challenge,
514 *Environ. Res. Lett.*, 13(6), doi:10.1088/1748-9326/aab9df, 2018.
- 515 Deines, J. M., Kendall, A. D. and Hyndman, D. W.: Annual Irrigation Dynamics in
516 the U.S. Northern High Plains Derived from Landsat Satellite Data, *Geophys.*
517 *Res. Lett.*, 44(18), 9350–9360, doi:10.1002/2017GL074071, 2017.
- 518 DeLucia, E. H., Chen, S., Guan, K., Peng, B., Li, Y., Gomez-Casanovas, N., Kantola,
519 I. B., Bernacchi, C. J., Huang, Y., Long, S. P. and Ort, D. R.: Are we
520 approaching a water ceiling to maize yields in the United States?, *Ecosphere*,
521 10(6), doi:10.1002/ecs2.2773, 2019.
- 522 Egli, D. B.: Seed- Fill Duration and Yield Of Grain Crops, *Adv. Agron.*, 83(C), 243–
523 279, doi:10.1016/S0065-2113(04)83005-0, 2004.
- 524 Elliott, J., Müller, C., Deryng, D., Chryssanthacopoulos, J., Boote, K. J., Büchner, M.,
525 Foster, I., Glotter, M., Heinke, J., Iizumi, T., Izaurralde, R. C., Mueller, N. D.,
526 Ray, D. K., Rosenzweig, C., Ruane, A. C. and Sheffield, J.: The Global Gridded
527 Crop Model intercomparison: data and modeling protocols for Phase 1 (v1.0),
528 *Geosci. Model Dev.*, 8, 261–277. <https://doi.org/10.5194/gmd-8-261-2015>
- 529 Felfelani, F., Pokhrel, Y., Guan, K. and Lawrence, D. M.: Utilizing SMAP Soil
530 Moisture Data to Constrain Irrigation in the Community Land Model, *Geophys.*
531 *Res. Lett.*, 45(23), 12,892–12,902, doi:10.1029/2018GL080870, 2018..

532 Gitelson, A. A.: Wide Dynamic Range Vegetation Index for Remote Quantification of
533 Biophysical Characteristics of Vegetation, *J. Plant Physiol.*, 161(2), 165–173,
534 doi:10.1078/0176-1617-01176, 2004.

535 Howell, T. A.: Enhancing water use efficiency in irrigated agriculture, *Agron J*, vol.
536 93, pp. 281–289., 2001.

537 Huryňa, H., Cohen, Y., Karnieli, A., Panov, N., Kustas, W. P. and Agam, N.:
538 Evaluation of TsHARP utility for thermal sharpening of Sentinel-3 satellite
539 images using Sentinel-2 visual imagery, *Remote Sens.*, 11(19),
540 doi:10.3390/rs11192304, 2019.

541 Jalilvand, E., Tajrishy, M., Ghazi Zadeh Hashemi, S. A. and Brocca, L.:
542 Quantification of irrigation water using remote sensing of soil moisture in a
543 semi-arid region, *Remote Sens. Environ.*, 231, doi:10.1016/j.rse.2019.111226,
544 2019.

545 Jin, Z., Zhuang, Q., Wang, J., Archontoulis, S. V., Zobel, Z. and Kotamarthi, V. R.:
546 The combined and separate impacts of climate extremes on the current and future
547 US rainfed maize and soybean production under elevated CO₂, *Glob. Chang.*
548 *Biol.*, 23(7), 2687–2704, doi:10.1111/gcb.13617, 2017.

549 Johnson, D. M.: A comprehensive assessment of the correlations between field crop
550 yields and commonly used MODIS products, *Int. J. Appl. Earth Obs. Geoinf.*,
551 52, 65–81, doi:10.1016/j.jag.2016.05.010, 2016.

552 Kang, S. and Eltahir, E. A. B.: Impact of Irrigation on Regional Climate Over Eastern
553 China, *Geophys. Res. Lett.*, 46(10), 5499–5505, doi:10.1029/2019GL082396,
554 2019.

555 Kar, G. and Kumar, A.: Surface energy fluxes and crop water stress index in
556 groundnut under irrigated ecosystem, *Agric. For. Meteorol.*, 146(1–2), 94–106,
557 doi:10.1016/j.agrformet.2007.05.008, 2007.

558 Ke, Y., Im, J., Park, S. and Gong, H.: Downscaling of MODIS One kilometer
559 evapotranspiration using Landsat-8 data and machine learning approaches,
560 *Remote Sens.*, 8(3), doi:10.3390/rs8030215, 2016.

561 Lawston, P. M., Santanello, J. A. and Kumar, S. V.: Irrigation Signals Detected From
562 SMAP Soil Moisture Retrievals, *Geophys. Res. Lett.*, 44(23), 11,860-11,867,
563 doi:10.1002/2017GL075733, 2017.

564 Li, Y., Guan, K., Yu, A., Peng, B., Zhao, L., Li, B. and Peng, J.: Toward building a
565 transparent statistical model for improving crop yield prediction: Modeling

566 rainfed corn in the U.S, *F. Crop. Res.*, 234, 55–65,
567 doi:10.1016/j.fcr.2019.02.005, 2019.

568 Loarie, S. R., Lobell, D. B., Asner, G. P., Mu, Q. and Field, C. B.: Direct impacts on
569 local climate of sugar-cane expansion in Brazil, *Nat. Clim. Chang.*, 1(2), 105–
570 109, doi:10.1038/nclimate1067, 2011.

571 Lobell D B, Bänziger M, Magorokosho C, et al. Nonlinear heat effects on African
572 maize as evidenced by historical yield trials[J]. *Nature climate change*, 2011,
573 1(1): 42-45.

574 Meerdink, S. K., Hook, S. J., Roberts, D. A. and Abbott, E. A.: The ECOSTRESS
575 spectral library version 1.0, *Remote Sens. Environ.*, 230,
576 doi:10.1016/j.rse.2019.05.015, 2019.

577 Meng, C. L., Li, Z. L., Zhan, X., Shi, J. C. and Liu, C. Y.: Land surface temperature
578 data assimilation and its impact on evapotranspiration estimates from the
579 common land model, *Water Resour. Res.*, 45(2), doi:10.1029/2008WR006971,
580 2009.

581 Messina, C. D., Podlich, D., Dong, Z., Samples, M. and Cooper, M.: Yield-trait
582 performance landscapes: From theory to application in breeding maize for
583 drought tolerance, *J. Exp. Bot.*, 62(3), 855–868, doi:10.1093/jxb/erq329, 2011.

584 Mu, Q., Zhao, M. and Running, S. W.: Improvements to a MODIS global terrestrial
585 evapotranspiration algorithm, *Remote Sens. Environ.*, 115(8), 1781–1800,
586 doi:10.1016/j.rse.2011.02.019, 2011.

587 Mu, Q., Zhao, M., Kimball, J. S., McDowell, N. G. and Running, S. W.: A remotely
588 sensed global terrestrial drought severity index, *Bull. Am. Meteorol. Soc.*, 94(1),
589 83–98, doi:10.1175/BAMS-D-11-00213.1, 2013.

590 Müller, C., Elliott, J., Kelly, D., Arneth, A., Balkovic, J., Ciais, P., Deryng, D.,
591 Folberth, C., Hoek, S., Izaurralde, R. C., Jones, C. D., Khabarov, N., Lawrence,
592 P., Liu, W., Olin, S., Pugh, T. A. M., Reddy, A., Rosenzweig, C., Ruane, A. C.,
593 Sakurai, G., Schmid, E., Skalsky, R., Wang, X., de Wit, A. and Yang, H.: The
594 Global Gridded Crop Model Intercomparison phase 1 simulation dataset, *Sci.*
595 *Data*, 6(1), doi:10.1038/s41597-019-0023-8, 2019.

596 Niu, J., Shen, C., Li, S. G. and Phanikumar, M. S.: Quantifying storage changes in
597 regional Great Lakes watersheds using a coupled subsurface-land surface process
598 model and GRACE, MODIS products, *Water Resour. Res.*, 50(9), 7359–7377,
599 doi:10.1002/2014WR015589, 2014.

600 Peng, S. S., Piao, S., Zeng, Z., Ciais, P., Zhou, L., Li, L. Z. X., Myneni, R. B., Yin, Y.
601 and Zeng, H.: Afforestation in China cools local land surface temperature, Proc.
602 Natl. Acad. Sci. U. S. A., 111(8), 2915–2919, doi:10.1073/pnas.1315126111,
603 2014.

604 Rosegrant, M.W., Cai, X. and Cline, S.: World Water and Food to 2025: Dealing
605 with Scarcity, Food Policy. <https://doi.org/10.1098/rstb.2005.1744>, 2002.

606 Ruiz-Vera, U.M., Siebers, M.H., Jaiswal, D., Ort, D.R. and Bernacchi, C.J.: Canopy
607 warming accelerates development in soybean and maize, offsetting the delay in
608 soybean reproductive development by elevated CO₂ concentrations. *Plant Cell*
609 *Environ.* 41, 2806–2820. <https://doi.org/10.1111/pce.13410>, 2018.

610 Running, S.W., Mu, Q., Zhao, M. and Moreno, A.: Modis Global Terrestrial
611 Evapotranspiration (ET) Product (NASA MOD16A2/A3) NASA Earth
612 Observing System Modis Land Algorithm. NASA: Washington, DC, USA.

613 Russo, S., Dosio, A., Graversen, R. G., Sillmann, J., Carrao, H., Dunbar, M. B.,
614 Singleton, A., Montagna, P., Barbola, P. and Vogt, J. V.: Magnitude of extreme
615 heat waves in present climate and their projection in a warming world, *J.*
616 *Geophys. Res. Atmos.*, 119(22), 12,500–12,512, doi:10.1002/2014JD022098,
617 2014.

618 Sacks, W. J., Cook, B. I., Buening, N., Levis, S. and Helkowski, J. H.: Effects of
619 global irrigation on the near-surface climate, *Clim. Dyn.*, 33(2–3), 159–175,
620 doi:10.1007/s00382-008-0445-z, 2009.

621 Sanchez, B., Rasmussen, A. and Porter, J.R. (2014). Temperatures and the growth and
622 development of maize and rice: a review. *Global Change Biology* 20, 408–417.

623 Senay, G. B., Bohms, S., Singh, R. K., Gowda, P. H., Velpuri, N. M., Alemu, H. and
624 Verdin, J. P.: Operational Evapotranspiration Mapping Using Remote Sensing
625 and Weather Datasets: A New Parameterization for the SSEB Approach, *J. Am.*
626 *Water Resour. Assoc.*, 49(3), 577–591, doi:10.1111/jawr.12057, 2013.

627 Siebert, S. and Döll, P.: Quantifying blue and green virtual water contents in global
628 crop production as well as potential production losses without irrigation, *J.*
629 *Hydrol.*, 384(3–4), 198–217, doi:10.1016/j.jhydrol.2009.07.031, 2010.

630 Siebert, S., Webber, H., Zhao, G. and Ewert, F.: Heat stress is overestimated in
631 climate impact studies for irrigated agriculture, *Environ. Res. Lett.*, 12(5),
632 doi:10.1088/1748-9326/aa702f, 2017.

633 Siebert, S., Ewert, F., Eyshi Rezaei, E., Kage, H. and Graß, R.: Impact of heat stress
634 on crop yield - On the importance of considering canopy temperature, *Environ.*
635 *Res. Lett.*, 9(4), doi:10.1088/1748-9326/9/4/044012, 2014.

636 Tack, J., Barkley, A. and Hendricks, N.: Irrigation offsets wheat yield reductions from
637 warming temperatures, *Environ. Res. Lett.*, 12(11), doi:10.1088/1748-
638 9326/aa8d27, 2017.

639 Teixeira, E. I., Fischer, G., Van Velthuisen, H., Walter, C. and Ewert, F.: Global hot-
640 spots of heat stress on agricultural crops due to climate change, *Agric. For.*
641 *Meteorol.*, 170, 206–215, doi:10.1016/j.agrformet.2011.09.002, 2013.

642 Teuling, A. J., Seneviratne, S. I., Stöckli, R., Reichstein, M., Moors, E., Ciais, P.,
643 Luysaert, S., Van Den Hurk, B., Ammann, C., Bernhofer, C., Dellwik, E.,
644 Gianelle, D., Gielen, B., Grünwald, T., Klumpp, K., Montagnani, L., Moureaux,
645 C., Sottocornola, M. and Wohlfahrt, G.: Contrasting response of European forest
646 and grassland energy exchange to heatwaves, *Nat. Geosci.*, 3(10), 722–727,
647 doi:10.1038/ngeo950, 2010.

648 Thiery, W., Davin, E. L., Lawrence, D. M., Hirsch, A. L., Hauser, M. and
649 Seneviratne, S. I.: Present-day irrigation mitigates heat extremes, *J. Geophys.*
650 *Res.*, 122(3), 1403–1422, doi:10.1002/2016JD025740, 2017.

651 Thornton, P. E., Thornton, M. M., Mayer, B. W., Wei, Y., Devarakonda, R., Vose, R.
652 S. and Cook, R. B.: Daymet: Daily Surface Weather Data on a 1-km Grid for
653 North America, Version 3, Version 3. ORNL DAAC, Oak Ridge, Tennessee,
654 USA [online] Available from: <https://search.earthdata.nasa.gov/search>, 2018.

655 Tomlinson, C. J., Chapman, L., Thornes, J. E. and Baker, C. J.: Derivation of
656 Birmingham’s summer surface urban heat island from MODIS satellite images,
657 *Int. J. Climatol.*, 32(2), 214–224, doi:10.1002/joc.2261, 2012.

658 Troy, T. J., Kipgen, C. and Pal, I.: The impact of climate extremes and irrigation on
659 US crop yields, *Environ. Res. Lett.*, 10(5), doi:10.1088/1748-9326/10/5/054013,
660 2015

661 US Department of Agriculture (USDA) NASS: Quick Stats: Agricultural Statistics
662 Data Base, Natl. Agric. Stat. Serv., Available from:
663 <http://www.nass.usda.gov/QuickStats/>, 2018a.

664 US Department of Agriculture (USDA): Crop Scape and Cropland Data Layer –
665 National Download.

666 https://www.nass.usda.gov/Research_and_Science/Cropland/Release/index.php.
667 2018b

668 Velpuri, N. M., Senay, G. B., Singh, R. K., Bohms, S. and Verdin, J. P.: A
669 comprehensive evaluation of two MODIS evapotranspiration products over the
670 conterminous United States: Using point and gridded FLUXNET and water
671 balance ET, *Remote Sens. Environ.*, 139, 35–49, doi:10.1016/j.rse.2013.07.013,
672 2013.

673 Wallace, J. S.: Increasing agricultural water use efficiency to meet future food
674 production, *Agric. Ecosyst. Environ.*, 82(1–3), 105–119, doi:10.1016/S0167-
675 8809(00)00220-6, 2000.

676 Wan, Z.: New refinements and validation of the MODIS Land-Surface
677 Temperature/Emissivity products, *Remote Sens. Environ.*, 112(1), 59–74,
678 doi:10.1016/j.rse.2006.06.026, 2008.

679 Wang, E. and Engel, T.: Simulation of phenological development of wheat crops,
680 *Agric. Syst.*, 58(1), 1–24, doi:10.1016/S0308-521X(98)00028-6, 1998.

681 Wang, F., Qin, Z., Song, C., Tu, L., Karnieli, A. and Zhao, S.: An improved mono-
682 window algorithm for land surface temperature retrieval from landsat 8 thermal
683 infrared sensor data, *Remote Sens.*, 7(4), 4268–4289, doi:10.3390/rs70404268,
684 2015.

685 Webber, H., Martre, P., Asseng, S., Kimball, B., White, J., Ottman, M., Wall, G. W.,
686 De Sanctis, G., Doltra, J., Grant, R., Kassie, B., Maiorano, A., Olesen, J. E.,
687 Ripoche, D., Rezaei, E. E., Semenov, M. A., Stratonovitch, P. and Ewert, F.:
688 Canopy temperature for simulation of heat stress in irrigated wheat in a semi-arid
689 environment: A multi-model comparison, *F. Crop. Res.*, 202, 21–35,
690 doi:10.1016/j.fcr.2015.10.009, 2017.

691 Xu, T., Liu, S., Liang, S. and Qin, J.: Improving predictions of water and heat fluxes
692 by assimilating MODIS land surface temperature products into the Common
693 Land Model, *J. Hydrometeorol.*, 12(2), 227–244, doi:10.1175/2010JHM1300.1,
694 2011.

695 Zaussinger, F., Dorigo, W., Gruber, A., Tarpanelli, A., Filippucci, P. and Brocca, L.:
696 Estimating irrigation water use over the contiguous United States by combining
697 satellite and reanalysis soil moisture data, *Hydrol. Earth Syst. Sci.*, 23(2), 897–
698 923, doi:10.5194/hess-23-897-2019, 2019.

699 Zhu, P., Jin, Z., Zhuang, Q., Ciaais, P., Bernacchi, C., Wang, X., Makowski, D. and
700 Lobell, D.: The important but weakening maize yield benefit of grain filling
701 prolongation in the US Midwest, *Glob. Chang. Biol.*, 24(10), 4718–4730,
702 doi:10.1111/gcb.14356, 2018.

703 Zhu, P., Zhuang, Q., Archontoulis, S. V., Bernacchi, C. and Müller, C.: Dissecting the
704 nonlinear response of maize yield to high temperature stress with model-data
705 integration, *Glob. Chang. Biol.*, 25(7), 2470–2484, doi:10.1111/gcb.14632,
706 2019.

707

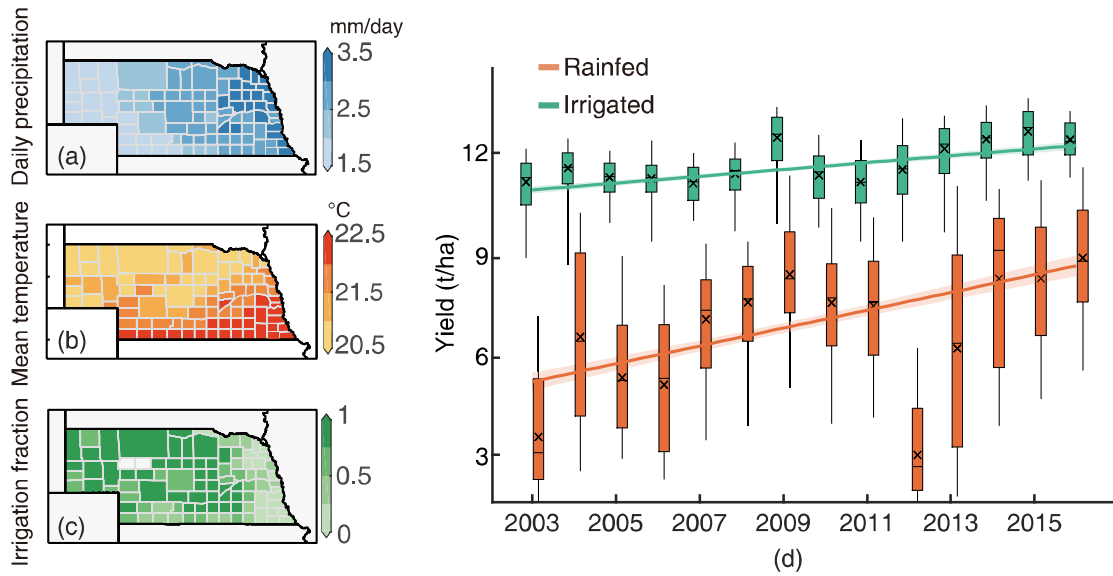
708 **Acknowledgments**

709

710 We thank the NSF/USDA NIFA INFEWS T1 #1639318 for funding support.

711

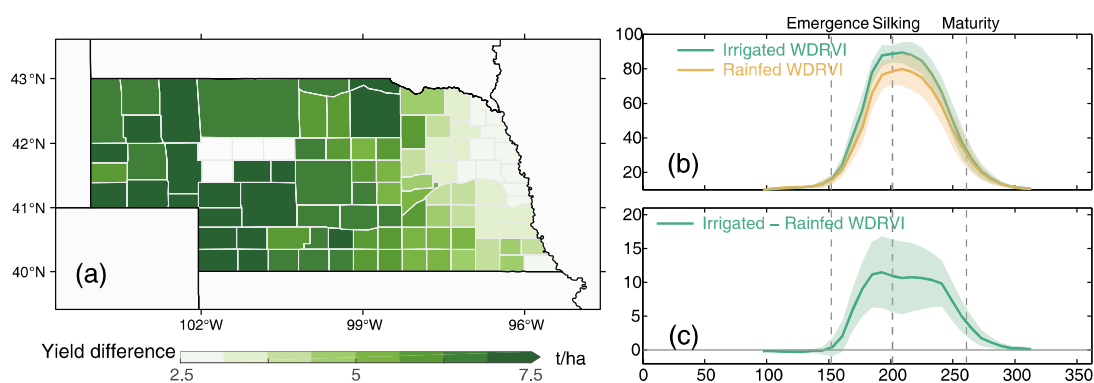
712 **Figures**



713

714 **Figure 1:** The spatial pattern of county level multi-year (2003-2016) mean daily
 715 precipitation (a) and air temperature (b) during maize growing season. County level
 716 multi-year (2003-2016) mean maize irrigation fraction across Nebraska (c). The
 717 maize irrigation fraction is based on USDA NASS report. Boxplot of county level
 718 irrigated and rainfed maize yield in Nebraska over the study period (d). The lines in (d)
 719 show the linear fitted yield trend with 95% confidence interval. Boxplots indicate the
 720 median (horizontal line), mean (cross), inter-quartile range (box), and 5–95th
 721 percentile (whiskers) of rainfed or irrigated yield across all counties.

722

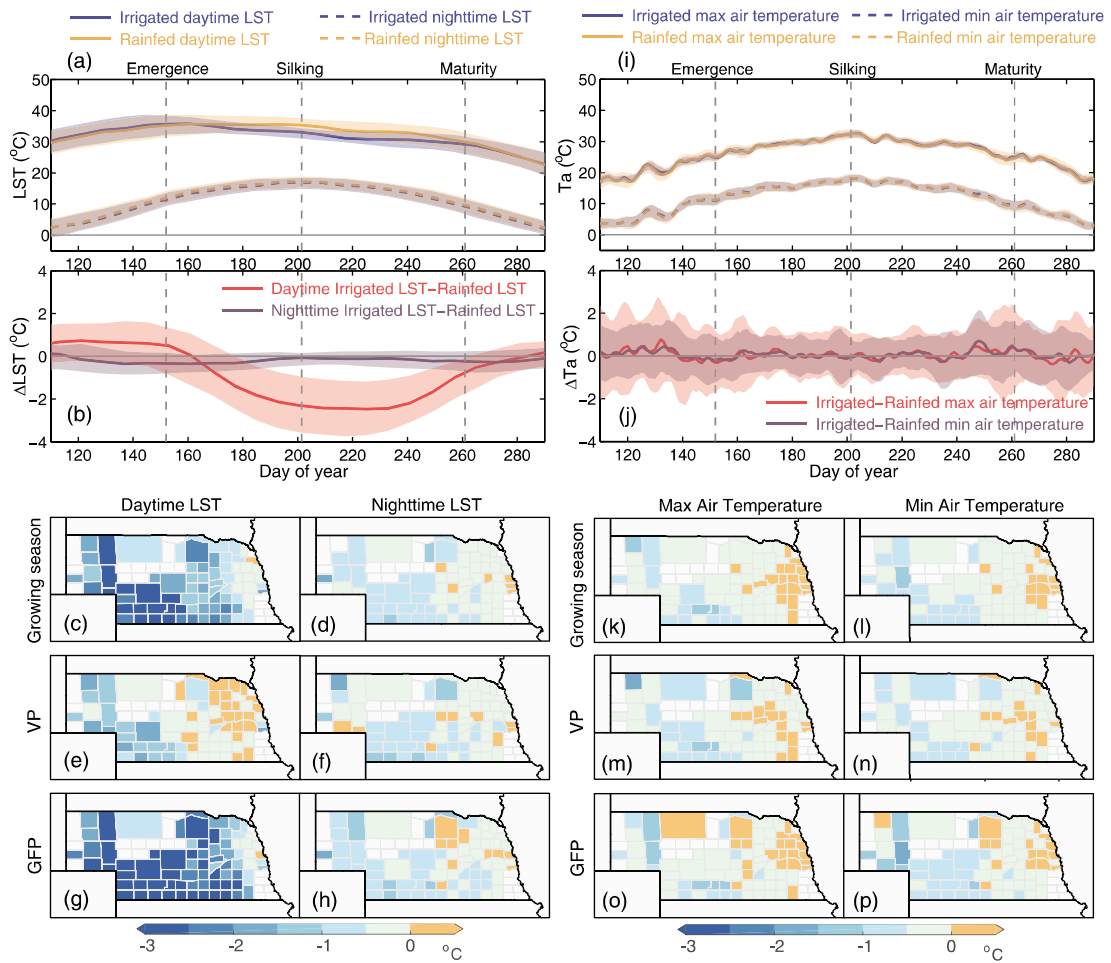


723

724 **Figure 2:** The difference between irrigated and rainfed maize yield (a) and satellite
 725 observed vegetation index (b and c). The shaded area in (b) and (c) shows one
 726 standard deviation of WDRVI (b) and WDRVI difference (c).

727

728

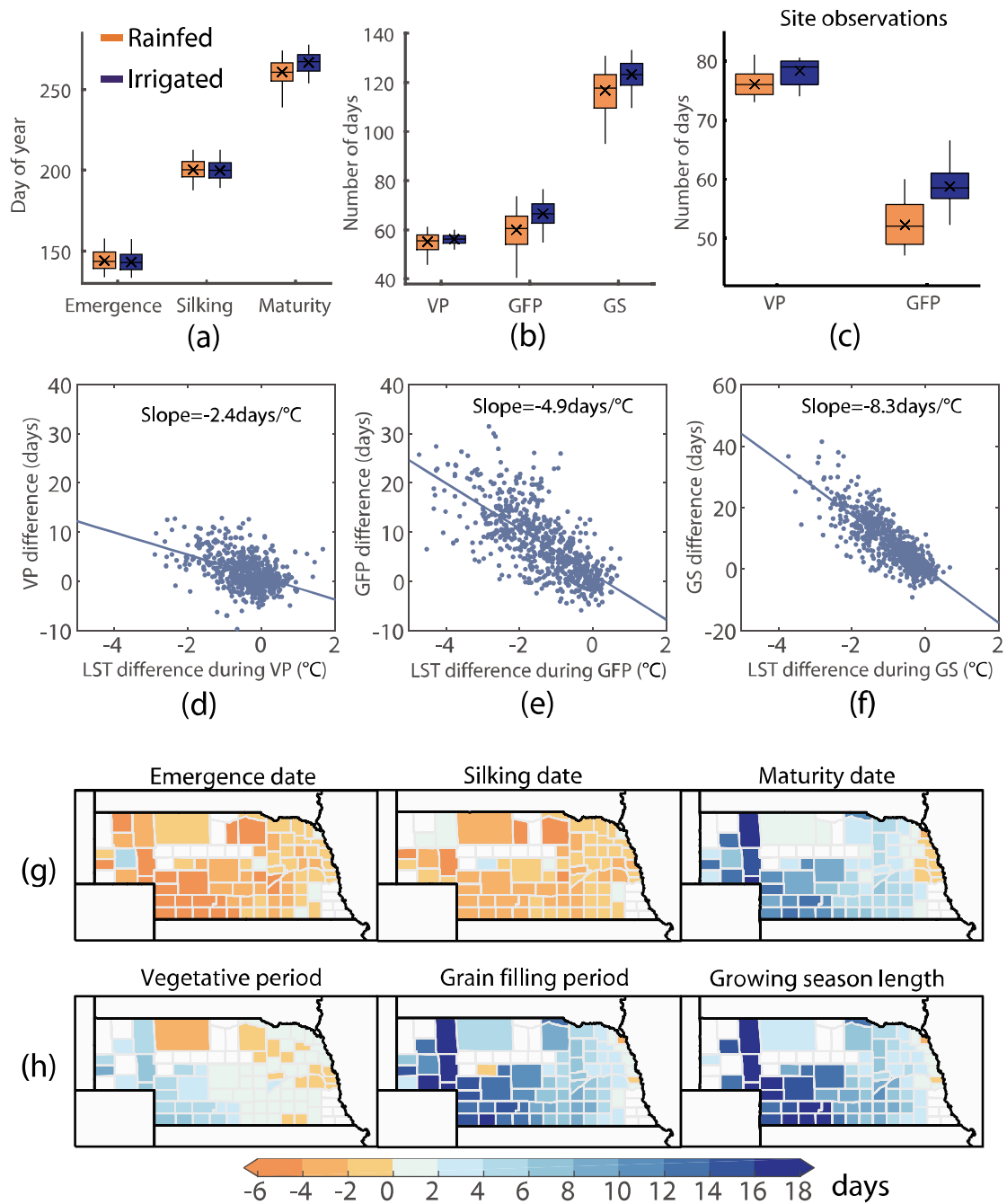


729

730 **Figure 3:** Spatial-temporal patterns of daytime and nighttime MODIS LST
 731 differences (left panel, a-h) and surface air temperature differences (right panel, i-p)
 732 between irrigated and rainfed maize in different growth stages: vegetative period and
 733 grain filling period. The shaded areas in (a), (b) and (i), (j) show one standard
 734 deviation of corresponding variables.

735

736



737

738 **Figure 4:** Boxplot of maize phenological date (a) and duration (b-c) for irrigated and

739 rainfed maize areas. Sensitivity of phenological duration difference between irrigated

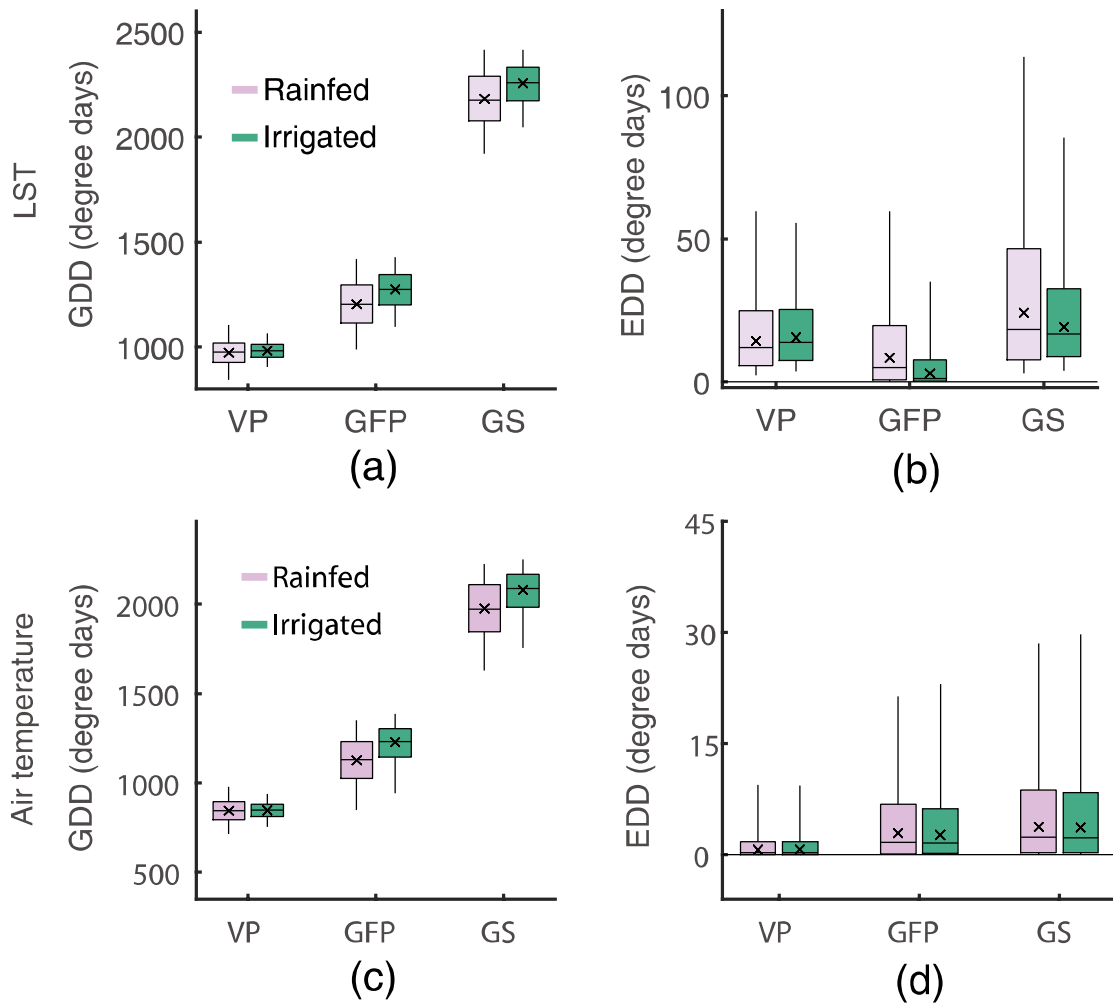
740 and rainfed maize to LST difference between irrigated and rainfed maize (d-f). The

741 slope in (d-f) was estimated with linear model. The spatial pattern of phenological

742 date and duration differences between irrigated and rainfed maize areas (g-h).

743

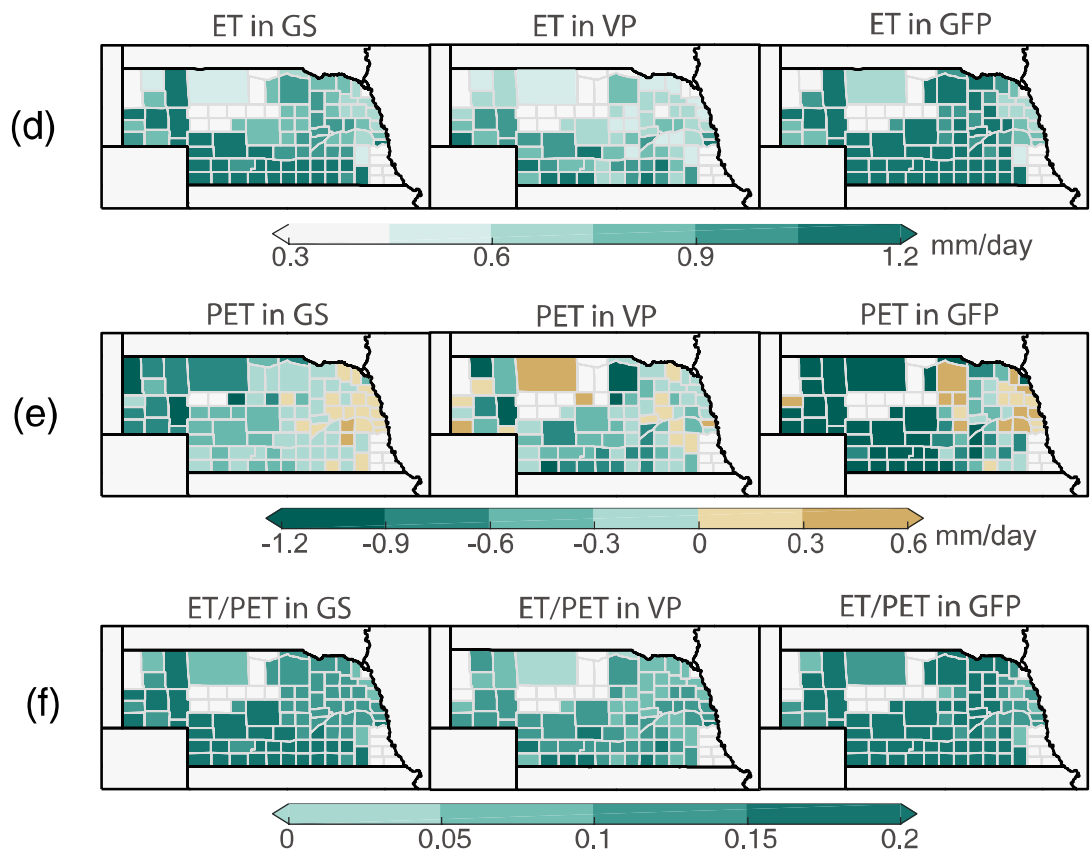
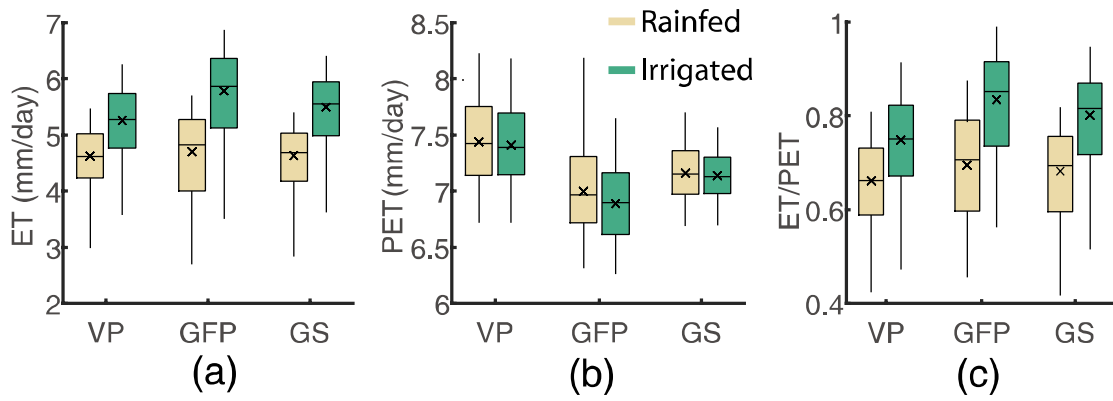
744



745

746 **Figure 5:** Boxplot of GDD and EDD estimated with MODIS LST (a-b) and surface
 747 air temperature (c-d) for irrigated and rainfed maize areas. Boxplots indicate the mean
 748 (cross), median (horizontal line), 25--75th percentile (box), and 5--95th percentile
 749 (whiskers) of corresponding variables in all year and county combinations.

750

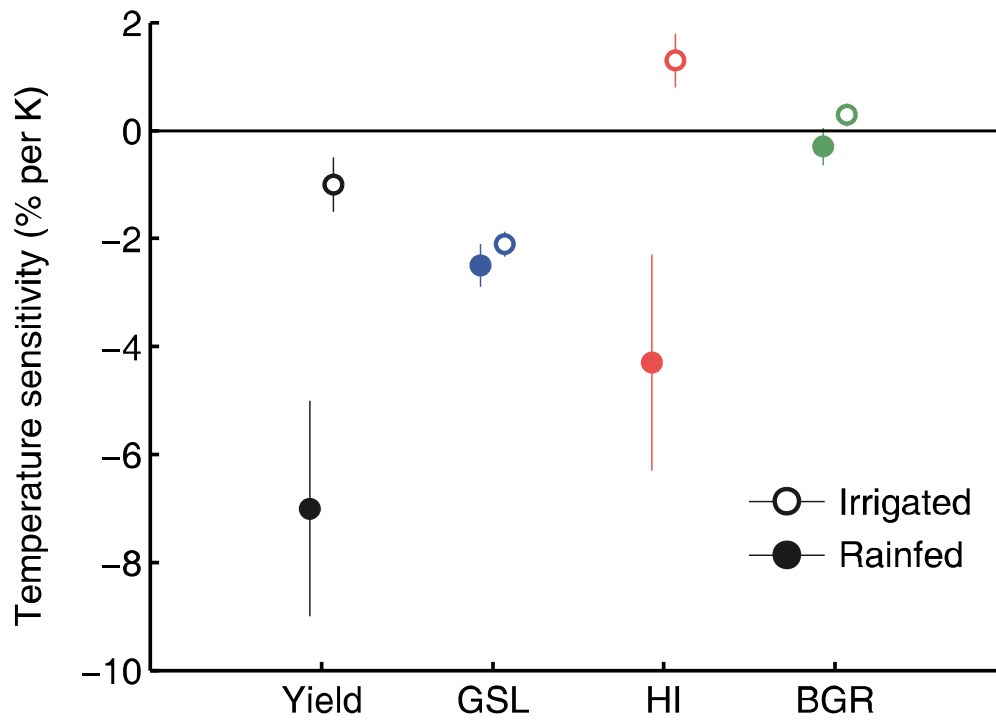


751

752

753 **Figure 6:** Boxplot of SSEBop ET, MODIS PET and ET/PET for irrigated and rainfed
 754 maize areas (a-c). Spatial pattern of SSEBop ET, MODIS PET and ET/PET
 755 differences between irrigated and rainfed maize areas (d-f).

756



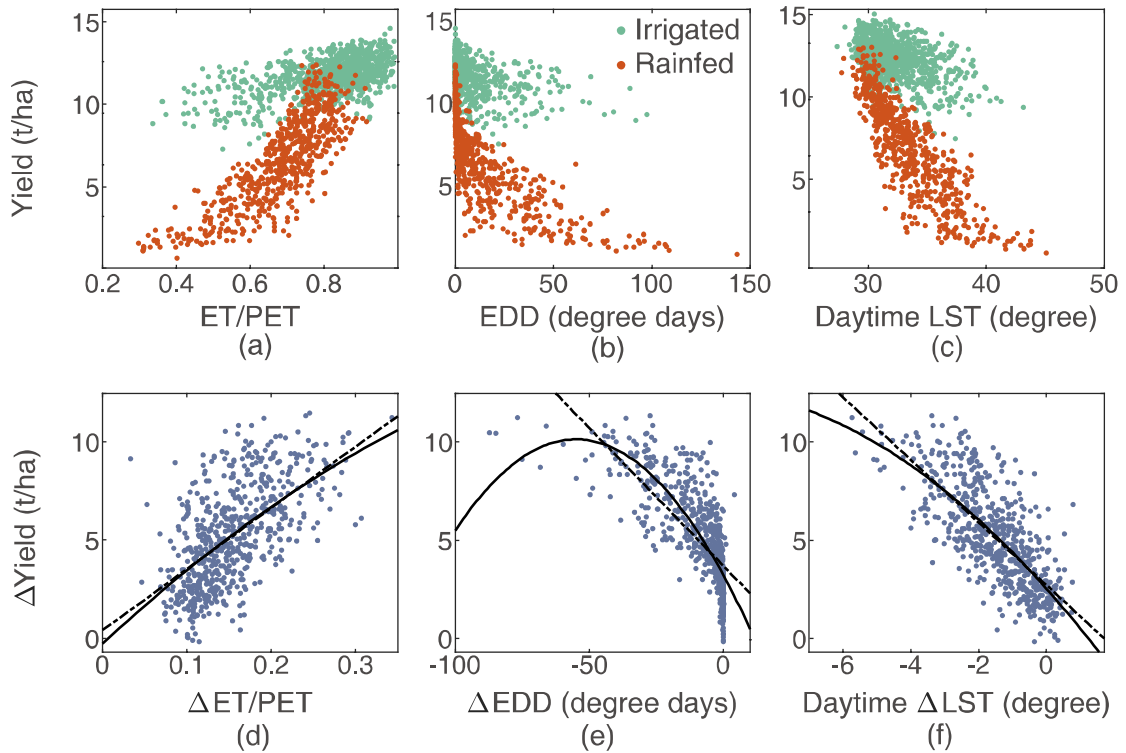
757

758 **Figure 7:** Temperature sensitivity of yield and yield components (GSL, HI and BGR)

759 for irrigated and rainfed maize areas.

760

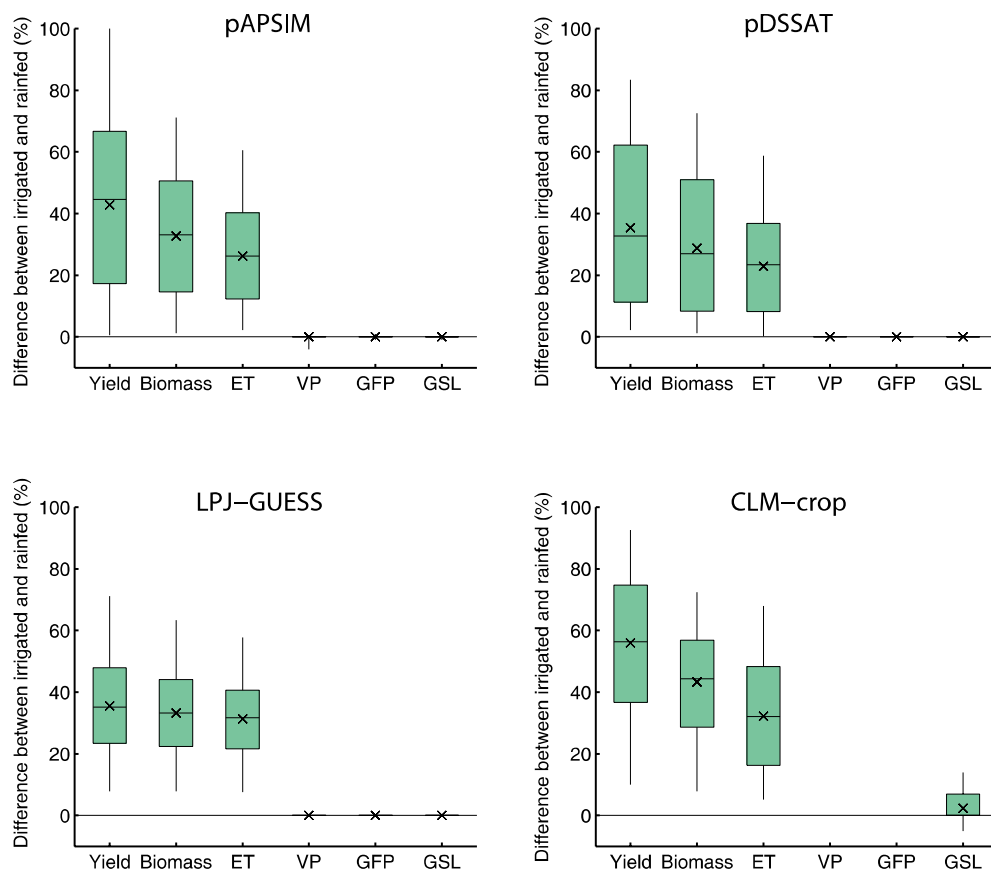
761



762

763 **Figure 8:** Response of maize yield to ET/PET (a), EDD (b) and daytime LST (c) in
 764 both irrigated and rainfed maize. Response of yield differences to ET/PET (d), EDD
 765 (e) and daytime LST (f) differences between irrigated and rainfed maize. The linear
 766 (dash black line) and quadratic (solid black line) response curves of $\Delta Yield$ to
 767 $\Delta ET/PET$, ΔEDD and ΔLST are shown in d-f.

768
 769
 770



771

772 **Figure 9:** Boxplot of crop model simulated yield, biomass, ET and phenological
 773 duration (VP, GFP and GSL) differences between irrigated and rainfed maize areas.
 774 For phenological duration, CLM-crop only reports GSL.